Water Research 308 (2027) 126911

Contents lists available at ScienceDirect

Water Research

journal homepage: www.elsevier.com/locate/watres

An inundation threshold regulates nitrate reduction pathways in mangrove sediments

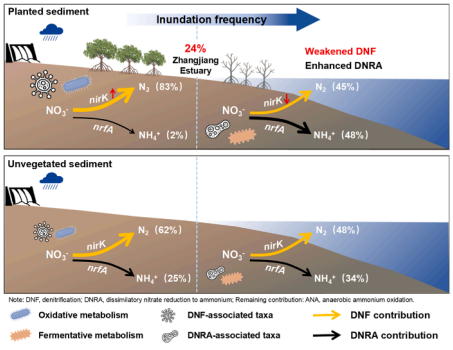
Shiyao Chen [a,b,c], Hui Wu [a,b,c], Yasong Chen [b], Fenfang Wang [d], Yihui Zhang [b], Nengwang Chen [a,b,c,*]

[a] Fujian Provincial Key Laboratory for Coastal Ecology and Environmental Studies, College of the Environment and Ecology, Xiamen University, Xiamen, 361102, China
[b] National Field Observation and Research Station (Fujian Taiwan Strait) for Marine Ecosystem, Xiamen University, Zhangzhou, 363300, China
[c] State Key Laboratory of Marine Environment Science, Xiamen University, Xiamen, 361102, China
[d] Polar and Marine Research Institute, College of Harbor and Coastal Engineering, Jimei University, Xiamen, 361021, China

HIGHLIGHTS

- A 24 % inundation threshold shifted nitrate fate in planted sediments only.
- The DNF–DNRA shift was far stronger in planted than unvegetated sediments.
- Plant failure lowered redox, enriching DNRA microbes, thus weakening N removal.

GRAPHICAL ABSTRACT



ARTICLE INFO

Keywords:
Hydrological regime
Nitrate removal
Denitrification
DNRA
Wetland
Estuary

ABSTRACT

Estuarine hydrological regimes are increasingly altered by dam operations and extreme climate events, reshaping inundation in intertidal wetlands. However, how inundation regulates nitrate (NO_3^-) fate remains unclear. We conducted an 18-month, elevation-controlled marsh-organ experiment with *Avicennia marina*-planted and unvegetated sediments across a 0 %–65 % gradient in mean inundation frequency. We combined ^{15}N isotope tracing and metagenomics to quantify NO_3^- reduction pathways and associated microbial attributes. In unvegetated sediments, increasing inundation reduced the contribution of denitrification (DNF) from 62 % to 48 % and increased dissimilatory nitrate reduction to ammonium (DNRA) from 25 % to 34 %. In planted sediments, NO_3^- reduction shifted nonlinearly at approximately 24 % mean inundation frequency. Below this threshold, DNF dominated, contributing 83 %–87 % of NO_3^- reduction, whereas DNRA contributed only 2 %–6 %. Above the threshold, DNF declined to 45 % at the highest inundation frequencies, while DNRA increased to 42 %–48 %, indicating a shift from nitrogen removal toward retention. This transition coincided with plant failure, more reducing conditions, and changes in microbial community and functional profiles. Plant survival was associated

* Corresponding author at: Fujian Provincial Key Laboratory for Coastal Ecology and Environmental Studies, College of the Environment and Ecology, Xiamen University, Xiamen, 361102, China.
E-mail addresses: shiyaochen@stu.xmu.edu.cn (S. Chen), wuhui@stu.xmu.edu.cn (H. Wu), yasongchen@foxmail.com (Y. Chen), ffwang@jmu.edu.cn (F. Wang), zyh@xmu.edu.cn (Y. Zhang), nwchen@xmu.edu.cn (N. Chen).

https://doi.org/10.1016/j.watres.2026.126911
Received 7 June 2026; Received in revised form 15 August 2026; Accepted 9 September 2026
Available online 9 September 2026
0043-1354/© 2026 Elsevier Ltd. All rights are reserved, including those for text and data mining, AI training, and similar technologies.

with DNF-related taxa (e.g., Pseudomonas and Flavobacterium), *nirK*, and oxidative metabolism, whereas plant failure was associated with DNRA-related taxa (e.g., Shewanella and Geobacter), *nrfA*, and fermentative metabolism. These findings identify a vegetation-dependent inundation threshold beyond which nitrogen removal declines and nitrogen retention increases in mangrove sediments.

1. Introduction

Intertidal mangrove wetlands are important nitrogen filters at the land–sea interface, where microbial transformations in anoxic sediments regulate the delivery of terrestrial nitrogen to estuarine and coastal waters (Nedwell, 1975). Nitrate (NO_3^-) can be reduced through denitrification (DNF) and dissimilatory nitrate reduction to ammonium (DNRA), while nitrate-derived nitrite may also support anaerobic ammonium oxidation (ANA) (Wilson and Megonigal, 2025; Zhang et al., 2023). The relative dominance of these pathways directly determines the ultimate fate of reactive nitrogen: whether it is converted into gaseous forms (N_2/N_2O) and permanently removed, or retained within the ecosystem as ammonium nitrogen (NH_4^+) (Ballantine et al., 2014; Burgin and Hamilton, 2007). Therefore, resolving the balance between DNF-mediated NO_3^- removal and DNRA-mediated nitrogen retention is essential for evaluating the nitrogen-filtering function of mangrove wetlands.

This nitrogen-filtering function of mangrove wetlands may be altered as dam operations and extreme climate events reshape tidal inundation regimes (Cai et al., 2019; Elsey-Quirk et al., 2019; Spencer et al., 2016; Tahsin et al., 2018). In intertidal wetlands, sediment elevation relative to the tidal frame governs inundation frequency, with lower elevations experiencing more frequent inundation and higher elevations remaining exposed for longer periods (Peng et al., 2018; Voss et al., 2013). Consequently, elevation-derived differences in inundation can strongly influence NO_3^- fate by reshaping sediment physicochemical conditions that regulate DNF–DNRA partitioning (Zhai et al., 2018). Previous studies have identified oxidation–reduction potential (ORP), carbon-to-nitrogen stoichiometry, salinity, sulfide accumulation, and organic carbon quality as key controls on pathway partitioning (Wilson and Megonigal, 2025; Zhao et al., 2025). In general, prolonged inundation lowers sediment ORP, restricts oxygen diffusion and nitrification-derived NO_3^- supply, and promotes anaerobic metabolism (Li et al., 2019). Yet the reported effects of flooding on NO_3^- fate remain inconsistent. Moderate inundation may promote DNF by delivering NO_3^- to sediments and creating anoxic microsites suitable for NO_3^- respiration, thereby enhancing nitrogen removal (Davidson and Seitzinger, 2006; Handler et al., 2022), whereas others show that chronic inundation under strongly reducing and sulfide-rich conditions shifts NO_3^- reduction toward DNRA and favors nitrogen retention (An and Gardner, 2002; Ma et al., 2025; Wilson and Megonigal, 2025). However, most existing studies have relied on static site comparisons or short-term manipulations (Zhijiang et al., 2020), leaving unresolved whether DNF–DNRA partitioning changes along an elevation-derived inundation frequency gradient.

Beyond hydrological forcing alone, vegetation persistence may further modify how inundation-driven sediment conditions are translated into NO_3^- reduction pathways (Booth et al., 2023). Living mangrove roots can modify sediment redox and substrate conditions through oxygen transport and root-derived carbon inputs (Cheng et al., 2020; Huang et al., 2026), generating micro-oxic and carbon-enriched niches that may favor the DNF process (Alldred and Baines, 2016; Koyama et al., 2025; Li et al., 2020). Excessive inundation can restrict oxygen diffusion, reduce root activity, and decrease plant survival and biomass accumulation (Liao, 2010). Failed or decaying plant tissues may further supply organic substrates to already reducing sediments, thereby promoting fermentative metabolism and altering electron flow during NO_3^- reduction (Kristensen et al., 2008; van den Berg et al., 2017a). Therefore, it remains unclear whether vegetation persistence modifies hydrologically driven DNF–DNRA shifts across progressive inundation gradients, particularly when inundation approaches or exceeds the range that allows plant survival.

To address this question, we conducted an 18-month in situ marsh-organ experiment across an elevation-derived inundation gradient, comparing Avicennia marina-planted and unvegetated sediments. By integrating physicochemical measurements, ^{15}N isotope tracing, and shotgun metagenomics, we asked: (1) whether progressive inundation alone redirects sediment NO_3^- fate from DNF-mediated removal toward DNRA-mediated retention; (2) whether plant survival under the same inundation gradient modifies this hydrologically driven pathway shift in planted sediments; and (3) which sediment and microbial factors are associated with hydrologically driven DNF–DNRA partitioning.

2. Materials and methods

2.1. Design and sampling of an in situ marsh-organ

To manipulate sediment inundation frequency under field conditions, we established an in situ marsh-organ experiment along an elevation gradient in the Zhangjiang Estuary, Fujian Province, China (23°56′37″ N, 117°22′43″ E; Fig. 1) (Gao et al., 2024). The study area is a subtropical, tide-dominated estuary with a regular semidiurnal tide, a mean tidal range of 2.32 m, and a maximum tidal range of 4.14 m (Wang et al., 2023). The experimental platform was located in an upper-estuary, low-salinity reach strongly influenced by riverine inputs, where the mean seawater salinity during the experimental period was 5.08 PSU (Wang et al., 2025).

The elevation range was designed to span and exceed the natural vertical distribution of mangroves in the Zhangjiang Estuary. Based on the local tidal range and the broader marsh-organ platform, six representative elevations were selected: −50, 0, 50, 100, 150, and 200 cm relative to mean sea level. Inundation frequency at each elevation was estimated from water-level records collected at 10-min intervals using paired pressure transducers, with one sensor installed at the reference low-elevation mesocosm and the other recording atmospheric pressure. Daily inundation frequency was defined as the proportion of valid water-level records during which each elevation remained submerged. Daily values were averaged over the experimental period to obtain the mean inundation frequency for each elevation treatment (Text S1). The six elevations corresponded to mean inundation frequencies of approximately 65 %, 47 %, 28 %, 12 %, 2 %, and 0 %, respectively (Fig. 1c). At each elevation, six PVC cylinders (inner diameter: 28.5 cm; height: 33 cm; total capacity: 33 L) were installed and filled with sediment collected from the adjacent tidal flat. Three mesocosms were planted with *Avicennia marina* (*A. marina*), and three were left unvegetated as controls. To allow seawater exchange, three small holes (1.5 mm in diameter) were drilled at the bottom of each cylinder.

The experiment was conducted from April 2023 to October 2024, covering two growing seasons (Fig. 1c; Text S1). This duration allowed us to capture both early seedling mortality under excessive inundation and longer-term biomass accumulation in surviving treatments. *A. marina* was selected as the focal mangrove species because it is a flood-tolerant pioneer species commonly found in tidally influenced estuarine habitats in subtropical China (Wang et al., 2020). *A. marina* bag-grown saplings (initial biomass: 1.91 ± 0.12 g plant^{-1}) were transplanted at the start of the experiment. During the observation period, seedlings were considered dead when all leaves had fallen, the main stem had withered or broken, and no new buds emerged. By day

120, seedling survival at the −50 and 0 cm elevations had declined to 0 %. Dead seedlings and their root residues were retained in the mesocosms after mortality and were allowed to decompose naturally. Accordingly, the planted treatments at −50 and 0 cm represented failed plant establishment with a potential plant-detritus legacy. At the final harvest, plants were separated into aboveground and belowground tissues, oven-dried at 60 °C for 72 h to constant weight, and weighed to determine aboveground biomass (AGB), belowground biomass (BGB), and total biomass (TB), expressed as g plant^{-1} (Fig. S1).

After 18 months under the elevation-controlled inundation-frequency gradient, sediments were collected at the final harvest for physicochemical analyses, potential nitrogen-transformation incubations, and microbial analyses. Bulk surface sediments (0–5 cm) were collected from each cylinder within 2 h of sediment emergence during low tide using a clean stainless-steel spatula and were immediately sealed in sterile polyethylene bags. Samples for microbial analyses were stored at −80 °C until DNA extraction, whereas fresh subsamples were used for physicochemical measurements and nitrogen transformation incubations. In situ seawater was also collected from a nearby tidal creek using collapsible sampling bags and then filtered through 0.7 μm GF/F filters (Whatman) (Table S1).

2.2. Sediment physicochemical measurements

Sediment water content (WC) was determined gravimetrically by freeze-drying fresh sediment samples to constant mass. Sediment porewater salinity was measured using a handheld salinity refractometer (MASTER-S/Millα, ATAGO, Japan) after porewater was extracted from fresh sediments by centrifugation. Sediment oxidation–reduction potential (ORP) was measured in situ using a soil redox potential meter (LT-OPW, China). Concentrations of NH_4^+-N and NO_3^--N in sediment extracts (1 M KCl) were quantified using a continuous-flow nutrient analyzer (AA3, SEAL Analytical, Germany). Dissolved organic carbon (DOC) in sediment extracts (0.5 M K_2SO_4) was measured with a TOC analyzer (TOC-VCPH, Shimadzu, Japan) (Lu et al., 2023).

2.3. Measurement of potential NO_3^- reduction rates

Rates of DNF, ANA, and DNRA were determined by the ^{15}N isotope-pairing technique (Hou et al., 2014; Yin et al., 2016). The collected fresh sediments were mixed with helium-purged in situ seawater at a 1:5 (sediments/water) ratio and then stirred to form slurries. The slurries were transferred into the 12-mL borosilicate vials (Exetainer, Labco), which were sealed with butyl rubber stoppers and pre-incubated at 25 °C for 96 h to remove residual O_2 and NO_3^-. Then, 100 μL of $^{15}NO_3^-$. solution (^{15}N, 95 %; 10 mM) was injected into each vial. Half of the vials were designated as initial samples and immediately preserved with 150 μL of $ZnCl_2$ solution (7 mol L^{-1}). The remaining samples were incubated for another 8 h and then stopped with 150 μL $ZnCl_2$ solution. The concentrations of $^{29}N_2$ and $^{30}N_2$ produced during the incubation were determined by membrane inlet mass spectrometry (Bay Instruments, Easton, MD, USA), and the rates of DNF and ANA were calculated by Eqs. (1)-(3).

$$P_{29} = A_{29} + D_{29} \quad (1)$$

$$D_{29} = P_{30} \times 2 \times (1 - F_N) \times F_N^{-1} \quad (2)$$

$$D_t = D_{29} + 2 \times P_{30} \quad (3)$$

where P_{29} is the total production rate of $^{29}N_2$ (μmol h^{-1} kg^{-1}); A_{29} and D_{29} are the rates of $^{29}N_2$ produced by ANA and DNF (μmol h^{-1} kg^{-1}); P_{30} means the production rate of $^{30}N_2$ (μmol h^{-1} kg^{-1}); F_N is the fraction of

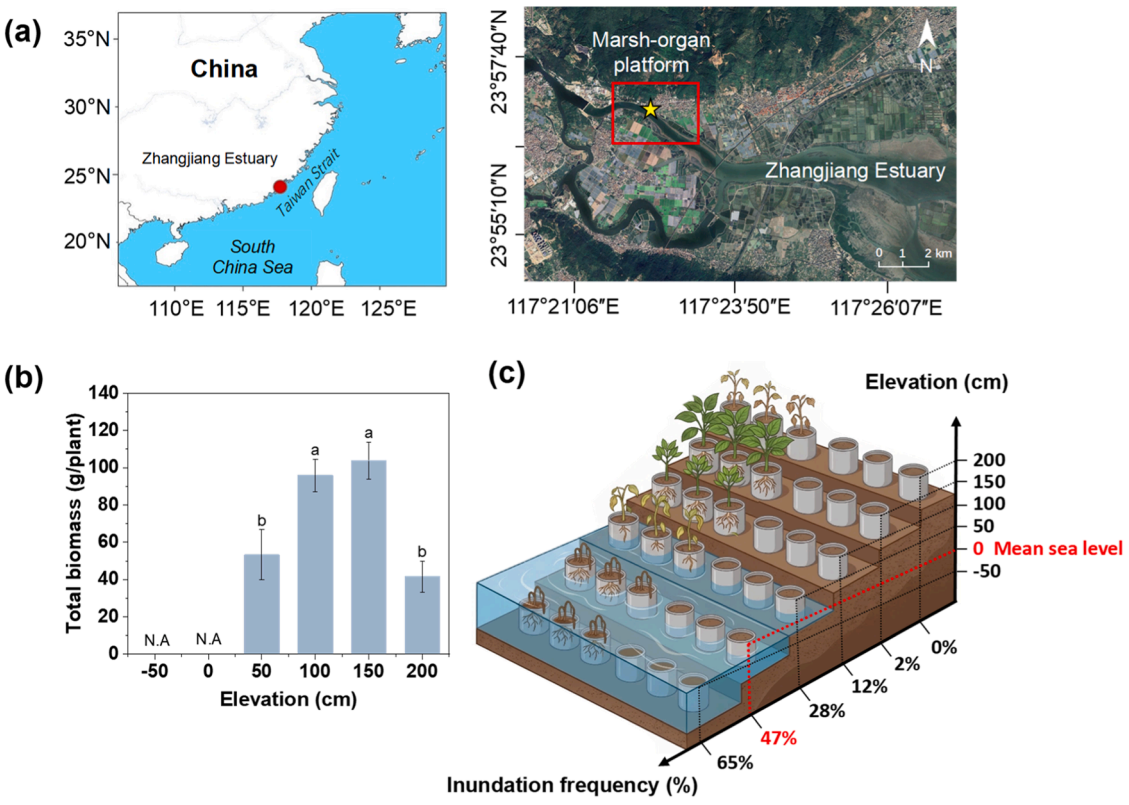


Fig. 1. Study area, sampling site, and experimental design. (a) Location of the study area and the marsh-organ platform in the upper Zhangjiang Estuary; (b) Changes in total biomass of *A.marina* along the elevation (inundation) gradient. Different lowercase letters indicate significant differences among treatments ($p < 0.05$). N.A. indicates no surviving plants at the −50 and 0 cm elevations; (c) Schematic representation of the in situ marsh-organ design across the elevation (inundation) gradient.

$^{15}NO_3^-$ in total NO_3^- (%); Dt is the total rate of DNF (μmol h^{-1} kg^{-1}).

Samples designated for DNRA analysis were transferred into 50 mL centrifuge tubes before measurement. Subsequently, they were flushed with helium again to remove the background $^{29}N_2$ and $^{30}N_2$ produced by DNF and ANA. Slurry was transferred into 12 mL glass vials, and the oxidizing agent was injected to oxidize $^{15}NH_4^+$. The dissolved $^{29}N_2$ and $^{30}N_2$ were measured using the method above.

The rate of DNRA was calculated by Eq. (4).

$$R_{DNRA} = \frac{\left[^{15}NH_4^+\right]_{final} {}^{*}V - \left[^{15}NH_4^+\right]_{initial} {}^{*}V}{W^{*}T} \quad (4)$$

where R_{DNRA} was the rate of DNRA (μmol N kg^{-1} h^{-1}), $[^{15}NH_4^+]_{initial}$ and $[^{15}NH_4^+]_{final}$ are the initial and final concentrations of $^{15}NH_4^+$ (μmol L^{-1}); V is the volume of glass vials (L); W means the dry weight of sediment in every glass vial (kg), and *T* is the incubation time.

2.4. DNA extraction and shotgun metagenomic sequencing

Genomic DNA was obtained from sediment samples with the HiPure Soil DNA Kit B (Magen, China). The purity of the extracted DNA was checked with a NanoDrop spectrophotometer, and the DNA concentration was determined using a Qubit 4 Fluorometer (Thermo Scientific, USA). Sequencing libraries that passed quality control were subsequently sequenced on the MGIseq-T7 platform, generating approximately 50 Gbp of paired-end data for each sample (Table S2).

Raw metagenomic reads were first processed with the Read_qc module implemented in metaWRAP (v1.3.2) to obtain clean reads (Uritskiy et al., 2018). Clean reads were assembled, and open reading frames were predicted before downstream annotation. Functional annotation and genus-level taxonomic profiling of predicted genes were performed using DIAMOND against KEGG and NCBI NR databases, respectively (Buchfink et al., 2015). DNF- and DNRA-related genes were identified from KEGG annotations. MAGs were reconstructed using multiple binning algorithms, quality-screened, dereplicated, taxonomically classified, and functionally annotated with METABOLIC (Zhou et al., 2022). MAGs carrying DNF- or DNRA-related marker genes were selected for genome-resolved analyses of nitrogen, carbon, and energy metabolism. Detailed bioinformatic parameters, normalization procedures, MAG quality criteria, and functional module definitions are provided in Text S2 and Table S3.

2.5. Statistical analyses

Values are presented as mean ± standard deviation (n = 3) for each elevation × planting treatment combination. Normality and homogeneity of variance were assessed using the Shapiro–Wilk and Levene's tests, respectively, and data were transformed when necessary. Effects of elevation, planting treatment (planted vs. unvegetated control), and their interaction on sediment properties and nitrogen transformation rates were tested using two-way ANOVA. Within each treatment, differences among elevations were assessed by one-way ANOVA followed by Tukey's HSD test, whereas planted–control differences at the same elevation were evaluated using Welch's *t*-tests with Holm correction. Plant biomass was analyzed separately across elevations where plants survived using one-way ANOVA followed by Tukey's HSD test. In addition to statistical significance, partial eta-squared (ηp^2) was calculated to quantify the effect sizes of elevation, planting treatment, and their interaction. All analyses were conducted in R 4.4.2, with significance set at $p < 0.05$.

To evaluate hydrological transitions, linear, quadratic, segmented, and four-parameter logistic models were compared using AICc and leave-one-inundation-level-out cross-validation. Transition uncertainty was assessed by bootstrap resampling. DNF - DNRA pathway balance was calculated as (DNF − DNRA)/(DNF + DNRA). Because only six inundation levels were available, transition estimates were interpreted as approximate.

Redundancy analysis (RDA) was performed using the relative abundances of the 28 key MAGs as response variables, with sediment physicochemical properties, nitrogen transformation rates, plant biomass, and carbon metabolic indices fitted as explanatory variables. Before RDA, all variables were standardized, and strongly collinear explanatory variables were screened using variance inflation factors (VIFs). The significance of the constrained ordination and explanatory variables was assessed using permutation tests.

A random forest model (RF) was constructed to evaluate the relative importance of environmental and microbial predictors for the contribution of DNF (DNF%). The model was implemented in R using the randomForest package, and variable importance was assessed using permutation-based increases in mean squared error. Based on the key predictors identified by the RF model, partial least squares structural equation modeling (PLS-SEM) was further applied to disentangle the direct and indirect effects of hydrological, physicochemical, plant, and microbial variables on pathway balance. Variables were standardized before model fitting. Path significance was evaluated using bootstrap resampling with 1000 resamples. Standardized path coefficients, 95 % confidence intervals, direct and indirect effects, and R^2 values of endogenous variables were used to evaluate the final model. R^2 values are reported in Table S5.

3. Results

3.1. Plant establishment and growth across the elevation gradient

The elevation gradient significantly affected mangrove establishment and growth (Fig. 1b and S1; $p < 0.05$). No plants survived at the −50 cm and 0 cm elevations, indicating that successful establishment occurred only at elevations ≥50 cm (0 %–28 % mean inundation frequency). From 50 cm to 150 cm, TB increased progressively, peaking at 150 cm (103.87 ± 10.02 g $plant^{-1}$), then declined at 200 cm (41.53 ± 8.49 g $plant^{-1}$). AGB and BGB followed the same pattern.

3.2. Changes in sediment physicochemical properties along the elevation gradient

Sediment physicochemical properties varied markedly along the elevation gradient (Fig. 2; Table 1). Two-way ANOVA showed that elevation had significant main effects on WC, ORP, NH_4^+-N, and DOC, whereas plant treatment significantly affected ORP, NH_4^+-N, and NO_3^--N. Significant elevation × plant interactions were detected for ORP and NH_4^+-N ($p < 0.001$).

Sediment WC declined with elevation in both treatments, whereas ORP increased markedly. WC declined from approximately 48 % at −50 cm to 24 %–27 % at 200 cm, with a significant difference between Plant and CK treatments detected only at 200 cm ($p < 0.001$). In planted sediments, ORP increased from −54.67 ± 5.18 mV at −50 cm to >280 mV at elevations ≥100 cm, while comparisons with the unvegetated controls showed lower ORP at 0 cm and higher ORP at 100 cm, with no significant treatment differences at the remaining elevations ($p > 0.05$). Sediment porewater salinity showed only minor variation along the elevation gradient in both planted and unvegetated sediments, remaining within a narrow range of 1–5 PSU (Fig. S3).

Inorganic nitrogen dynamics varied distinctly. NO_3^--N concentrations remained consistently low (1.04–2.19 mg kg^{-1}) across the elevation gradient and showed no significant elevational trend ($p > 0.05$). NH_4^+-N showed a nonlinear response to elevation with a significant elevation × planting interaction. In planted sediments, concentrations were highest at −50 cm (6.57 ± 3.05 mg kg^{-1}), decreased sharply at 0 cm (2.17 ± 0.07 mg kg^{-1}), and remained relatively low at higher elevations. In unvegetated controls, NH_4^+-N varied across elevations and peaked at 50 cm (8.78 ± 2.83 mg kg^{-1}). Planted sediments had significantly lower NH_4^+-N than controls at 100, 150, and 200 cm ($p < 0.05$), with no

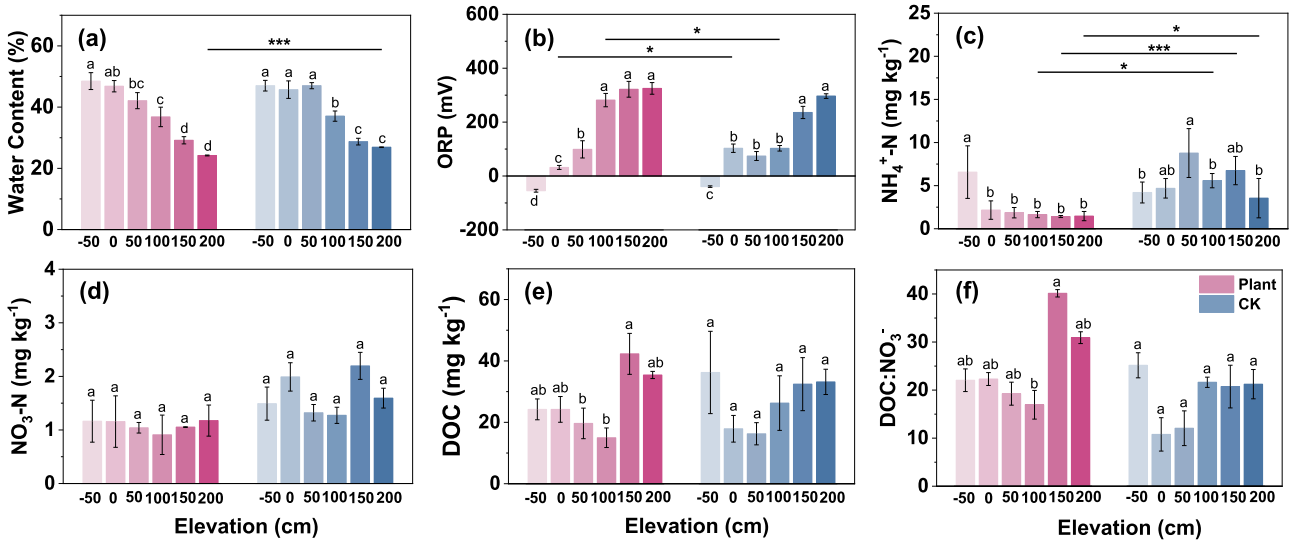


Fig. 2. Changes in sediment physicochemical properties across the elevation (inundation) gradient. Variations in sediment water content (a), ORP (b), NH_4^+-N (c), NO_3^--N (d), DOC (e), and the DOC: NO_3^- ratio (f) across elevation treatments. Plant and CK denote planted and unvegetated sediments (control), respectively. (*$p < 0.05$, **$p < 0.01$, and ***$p < 0.001$).

Table 1
Main effect and interaction effect of elevation and plant on sediment physicochemical properties and nitrogen transformation rates.

	Elevation			Plant			Elevation × Plant		
	F	P	ηp^2	F	P	ηp^2	F	P	ηp^2
Water Content	140.02	<0.001	0.967	1.50	0.233	0.059	2.46	0.062	0.339
ORP	354.98	<0.001	0.987	27.83	<0.001	0.537	30.89	<0.001	0.866
NH_4^+-N	4.81	<0.01	0.500	42.50	<0.001	0.639	7.97	<0.001	0.624
NO_3^--N	0.79	0.567	0.141	8.19	<0.01	0.254	0.55	0.736	0.103
DOC	3.16	0.025	0.397	0.01	0.919	<0.001	1.03	0.423	0.177
DOC: NO_3^-	2.23	0.084	0.317	4.21	0.051	0.149	1.43	0.250	0.229
DNF Rate	34.37	<0.001	0.877	602.37	<0.001	0.962	74.24	<0.001	0.939
DNRA Rate	212.09	<0.001	0.978	46.49	<0.001	0.660	13.07	<0.001	0.731
ANA Rate	2.48	0.061	0.341	0.06	0.802	0.002	6.26	<0.001	0.566

significant treatment differences at −50, 0, or 50 cm ($p > 0.05$).

DOC varied with elevation mainly in planted sediments, increasing from 14.97 to 24.22 mg kg^{-1} at −50 to 100 cm to 42.31 ± 11.57 mg kg^{-1} at 150 cm. No significant elevation effect was observed in controls ($p > 0.05$), and Plant–CK differences were not significant at individual elevations. The DOC: NO_3^- ratio showed no significant overall elevation or planting effect, although it peaked at 150 cm in planted sediments (40.14 ± 10.77 mg kg^{-1}) and exceeded the value at 100 cm (16.95 ± 2.99 mg kg^{-1}).

3.3. Potential rates of NO_3^- reduction pathways

Potential NO_3^- reduction rates differed significantly along the elevation gradient (Fig. 3; Table 1). Potential DNF rates showed opposing trends between the two treatments along the elevation gradient (Fig. 3a). In the CK group, DNF rates decreased with elevation, peaking at −50 cm (3.23 ± 0.14 μmol h^{-1} kg^{-1}) and dropping notably above 100 cm. Conversely, DNF rates in the planted sediments increased with elevation, starting from a minimum at −50 cm (3.93 ± 0.02 μmol h^{-1} kg^{-1}) and reaching a peak at 150 cm (12.25 ± 0.17 μmol h^{-1} kg^{-1}). Differences between the two treatments were highly significant across most elevations ($p < 0.001$).

Potential ANA rates were generally low and showed a treatment-dependent unimodal pattern along the elevation gradient (Fig. 3b). In the CK treatment, ANA rates peaked at 0 cm (2.05 ± 0.19 μmol h^{-1} kg^{-1}), whereas in the planted treatment, the peak occurred at 150 cm (2.11 ± 0.71 μmol h^{-1} kg^{-1}). At the lower elevations (−50 and 0 cm), ANA rates were slightly higher in the CK treatment than in the planted treatment, whereas at higher elevations (150–200 cm), planted sediments tended to show slightly higher ANA rates than the CK treatment.

Potential DNRA rates were highest under the most strongly flooded conditions (−50 cm), where planted sediments exhibited higher rates (3.38 ± 0.29 μmol h^{-1} kg^{-1}) than the CK treatment (2.52 ± 0.28 μmol h^{-1} kg^{-1}). DNRA rates then declined rapidly with increasing elevation, approaching zero above 50 cm. No significant differences between planted and unvegetated sediments were observed at the 100–200 cm elevations (Fig. 3c; $p > 0.05$).

Across the elevation gradient, DNF contribution increased whereas DNRA contribution declined with increasing elevation, and this divergence was stronger in planted than unvegetated sediments (Fig. 3d and S2). Specifically, unvegetated sediments at lower elevations (<50 cm) were relatively more DNRA-oriented, with DNF contributing approximately 43 %–48 % and DNRA 28 %–34 % of total NO_3^- reduction. Above 50 cm, the contribution of DNF increased from about 48 % to nearly 65 %, whereas DNRA declined to 11 %–25 %. In planted sediments, DNRA reached 42 %–48 % at the −50 and 0 cm elevations, where A. marina did not survive, but declined to 2 %–6 % at elevations ≥50 cm, where plants survived; correspondingly, DNF contribution increased from approximately 63 % to 85 %. ANA contributed approximately 7 %–15 % of total potential NO_3^- reduction in planted sediments and 13 %–23 % in unvegetated controls. These contributions were comparable to those reported for other estuarine and tidal-wetland sediments (Table S8).

Effect-size analysis further showed that the relative importance of

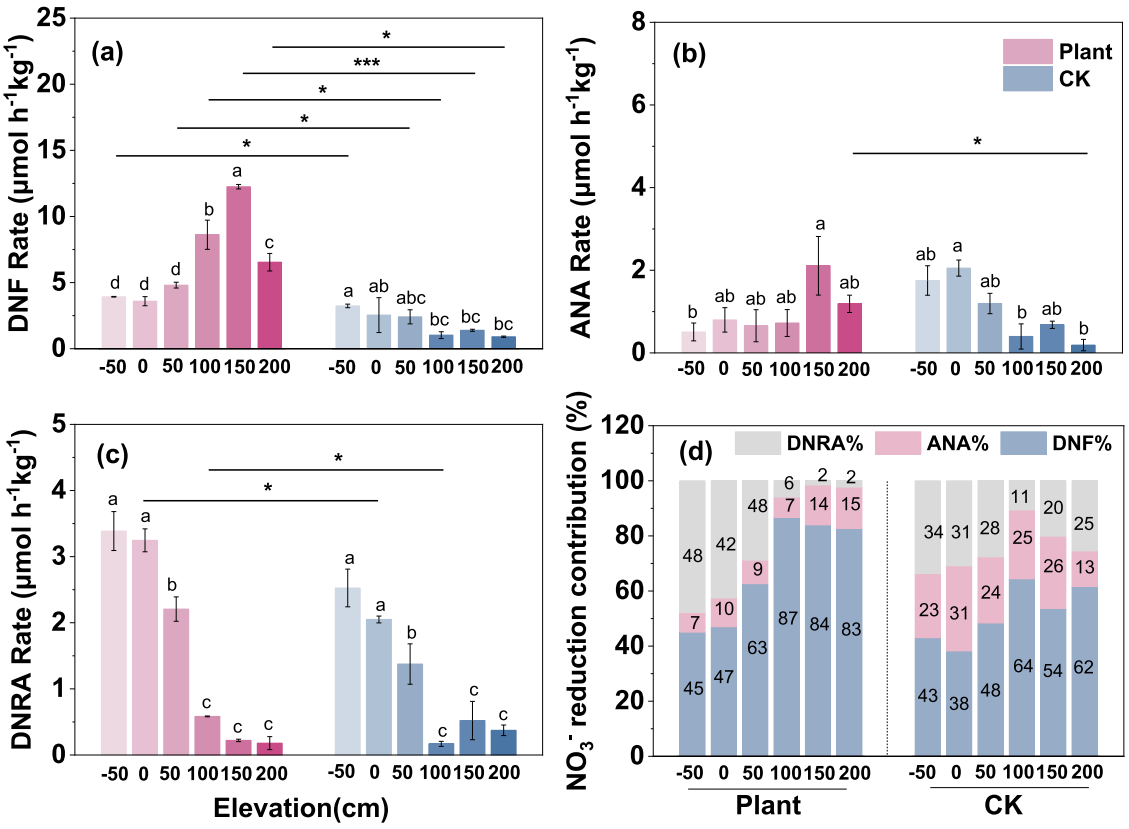


Fig. 3. Potential rates and relative contributions of NO_3^- reduction pathways across the elevation (inundation) gradient. Variations in potential DNF rates (a), ANA rates (b), DNRA rates (c), and the relative contributions of DNF, ANA, and DNRA (d) across elevation treatments. Plant and CK denote planted and unvegetated sediments (control), respectively. Different lowercase letters indicate significant differences among elevations within each treatment, whereas asterisks indicate significant differences between Plant and CK at the same elevation (*p < 0.05, **p < 0.01, and ***p < 0.001).

elevation and planting differed among nitrogen-transformation pathways (Table 1). Planting exerted the strongest effect on potential DNF ($\eta p^2 = 0.962$), whereas elevation showed the strongest effect on DNRA ($\eta p^2 = 0.978$). A substantial elevation × planting interaction was also observed for DNF ($\eta p^2 = 0.939$), indicating that the planting effect varied strongly across the hydrological gradient.

3.4. Functional microbial taxa for NO_3^- transformation pathways

Taxonomic analysis at the genus level revealed clear shifts in microbial groups associated with NO_3^- reduction along the inundation gradient (Fig. 4a and b). In unvegetated sediments, the relative abundance of DNF-associated genera varied from 1.88 % to 2.38 % across elevations. In planted sediments, their relative abundance increased from 2.40 %–2.60 % at −50–0 cm to 4.40 %–8.20 % at 50–150 cm and peaked at 8.20 % at 150 cm, representing a 3.15-fold increase relative to −50 cm. At 150 cm, Pseudomonas, Paracoccus, Bacillus, and Flavobacterium together accounted for 73.17 % of the selected DNF-associated genera. In contrast, the relative abundance of DNRA-associated genera was highest at −50 cm, reaching 2.30 % in planted sediments and 1.54 % in unvegetated controls, and declined to 0.20 %–1.00 % at 100–200 cm. Shewanella, Geobacter, Aeromonas, and Clostridium collectively represented 69.6 % of the selected DNRA-associated genera at −50 cm in planted sediments.

Functional genes involved in NO_3^- transformation varied across treatments and elevations (Fig. 4c and d). In planted sediments, NO_3^- reduction genes, including *napA, narG, and narH*, were broadly abundant across the elevation gradient. At 100–200 cm, nirK, nirS, and nosZ abundances were 0.9–1.4 fold higher in planted sediments than in the corresponding unvegetated controls. By contrast, nrfA abundance at −50 and 0 cm was 1.16-fold and 1.03-fold higher, respectively, in planted sediments than in the controls.

To gain a deeper mechanistic understanding of the microbial communities driving these two pathways, we further examined the relevant functional genes at the genome-resolved level (Fig. 4e and Table S3). A total of 28 MAGs carrying genes involved in NO_3^- reduction were identified, including 15 MAGs containing key genes associated with one or more steps of DNF and 13 MAGs containing genes linked to DNRA. The combined abundance of DNRA-associated bins 18, 19, 20, 21, and 25 was 2.06–72.8 -fold higher under the −50–0 cm treatments than at 100–200 cm. In contrast, three MAGs within the DNF assemblages (bin4, bin7, and bin9, belonging toBacteroidota, Thermodesulfobacteriota, and Gemmatimonadota) exhibited exceptionally high abundances at 150 cm elevation.

Functional profiling revealed contrasting metabolic potentials between DNF- and DNRA-associated MAGs (Fig. 5; Tables S4). H_2-metabolism genes were detected in 46.2 % of DNRA-associated MAGs versus 13.3 % of DNF-associated MAGs, while acetate/ethanol-related functions occurred in 38.5 % versus 20.0 %, respectively. Formate-related functions occurred in both groups (38.5 %vs. 53.3 %), whereas respiratory and oxidative energy-metabolism modules were more frequently represented among DNF-associated MAGs. Several DNRA-associated MAGs also contained sulfur-metabolism functions.

3.5. Environmental and microbial correlates of DNF–DNRA partitioning

To elucidate the primary environmental factors and metabolic processes driving the bifurcation of NO_3^- reduction pathways, RDA was performed using the relative abundances of the 28 DNF- and DNRA-associated MAGs as response variables, while physicochemical

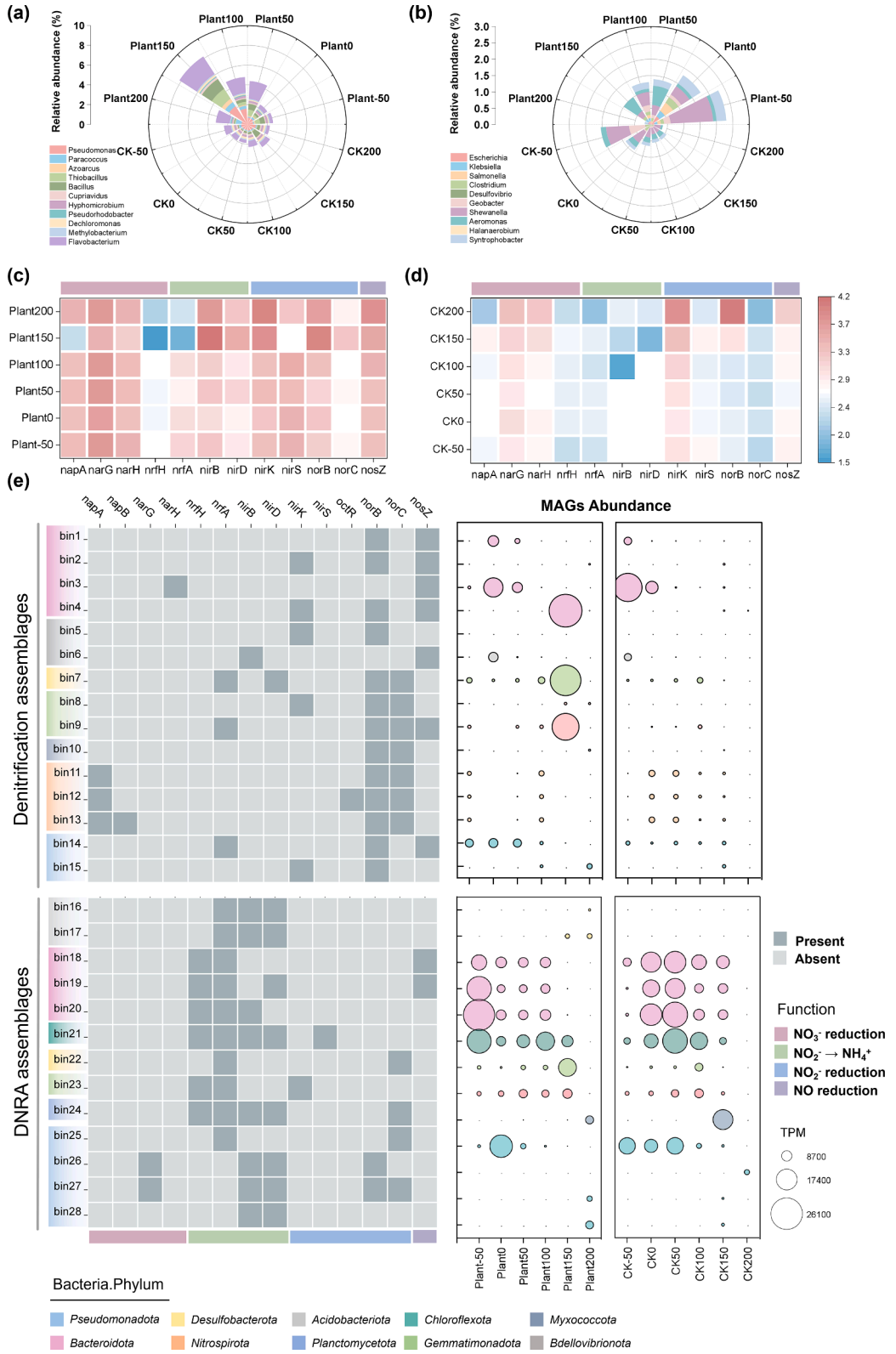


Fig. 4. DNF- and DNRA-associated functional microorganisms in planted and unvegetated sediments across elevation (inundation) gradient. Genus-level relative abundances of DNF-associated communities (a) and DNRA-associated communities (b) in planted and unvegetated sediments along the elevation-derived inundation gradient. Heatmaps showing the abundances of functional genes involved in NO_3^- reduction pathways in planted (c) and unvegetated sediments (d). Gene abundances were log_{10}-transformed and normalized. (e) Genome-resolved overview of 28 metagenome-assembled genomes (MAGs) associated with DNF and DNRA. Colors indicate the taxonomic affiliations of the MAGs, and the bar plot shows MAG contamination levels. The presence–absence matrix indicates nitrate-transformation genes encoded by each MAG, with gray cells denoting gene presence. The bubble plot shows the relative abundance of these MAGs across elevation treatments in planted and unvegetated sediments.

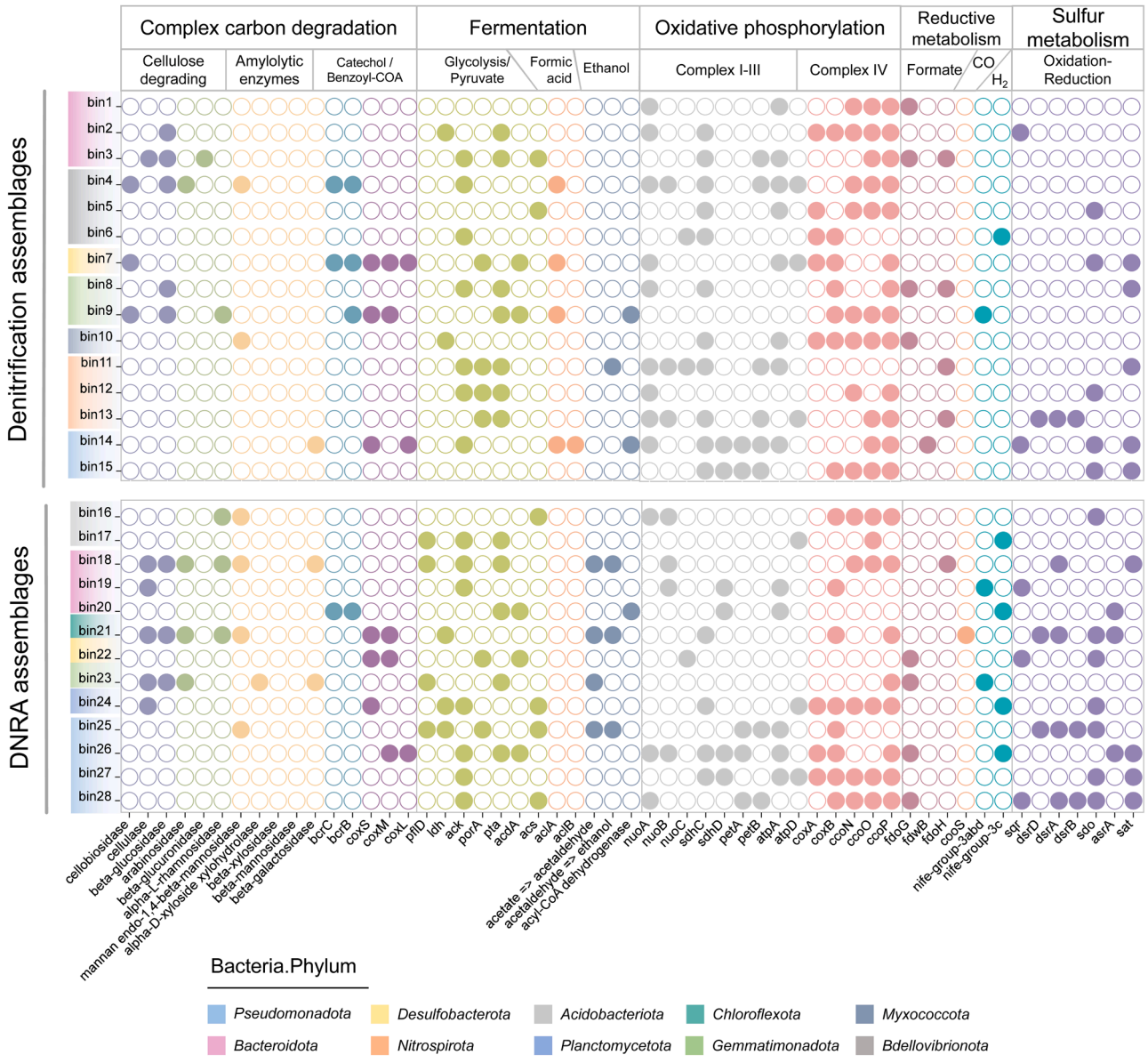


Fig. 5. Distribution of genes involved in carbon degradation, energy metabolism, and sulfur metabolism in denitrification (DNF)- and dissimilatory nitrate reduction to ammonium (DNRA)-associated MAGs. Colors denote distinct metabolic processes. Filled and open circles indicate gene presence and absence, respectively.

variables, nitrogen transformation rates, plant biomass, and metabolic indices were fitted as explanatory variables. The ordination suggested clear differentiation between microbial groups associated with DNF and DNRA. Specifically, the relative contribution of DNF% and DNF-associated MAGs was significantly and positively correlated with plant biomass and closely aligned with vectors representing oxidative metabolic processes (e.g., acetate oxidation). DOC was also closely coupled with major DNF MAGs and oxidative carbon utilization pathways. In sharp contrast, DNRA rates and principal DNRA-associated MAGs clustered tightly on the ordination plot, showing strong associations with highly reducing environmental characteristics and fermentative metabolic pathways (e.g., formate oxidation, ethanol oxidation, and hydrogen generation). Furthermore, the ORP exhibited distinct correlations with microbial fermentation, methane oxidation, and formaldehyde oxidation indices.

To quantify the relative importance of these regulators, a Random Forest model was constructed to predict DNF% (Fig. 6b). The model identified sediment ORP, WC, elevation, and plant presence as the variables with the highest predictive importance, together explaining a substantial fraction of the variation in DNF%. The *nirK:nrfA* ratio showed lower predictive importance and contributed less to model accuracy.

PLS-SEM further showed that hydrological and plant-related factors were associated with DNF–DNRA pathway balance (Fig. 6c,d; Table S5). The model explained 74.3 % of the variation in pathway balance. Mean inundation frequency was strongly associated with higher sediment water content ($\beta = 0.889$, $p < 0.001$), which was negatively associated with redox status ($\beta = -0.825$, $p < 0.001$) and pathway balance ($\beta = -0.692$, $p < 0.05$). In contrast, plant biomass was positively associated with both redox status ($\beta = 0.246$, $p < 0.001$) and pathway balance ($\beta = 0.445$, $p < 0.001$).

4. Discussion

4.1. High inundation weakens DNF dominance in unvegetated sediments

The unvegetated treatment provided a reference for evaluating the hydrological regulation of NO_3^- reduction partitioning in the absence of

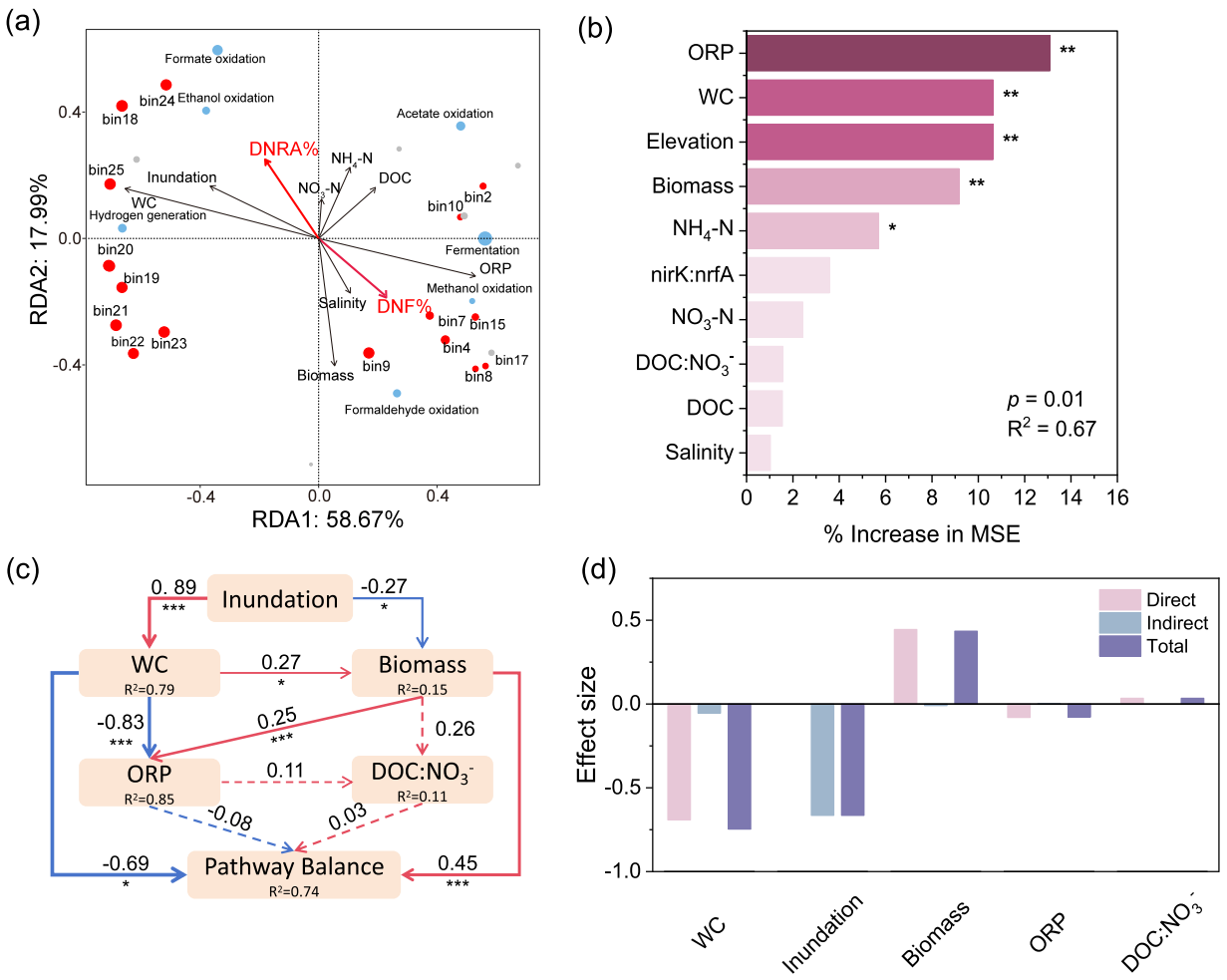


Fig. 6. Key environmental and microbial drivers regulating NO3- reduction pathway partitioning. (a) RDA of the relative abundances of 28 DNF- and DNRA-associated MAGs, NO3- reduction rates, carbon metabolism indices, and environmental variables. (b) Random forest analysis of predictor importance for DNF%. (c) PLS-SEM of direct and indirect associations among inundation, sediment properties, plant biomass, and DNF - DNRA pathway balance. (d) Direct, indirect, and total effects of key predictors on pathway balance. Numbers indicate standardized path coefficients. Solid and dashed paths indicate significant and non-significant associations, respectively; asterisks denote path significance. PLS-SEM, partial least squares structural equation modeling; DNF, denitrification; DNRA, dissimilatory nitrate reduction to ammonium.

plant effects (Fig. 3 & S2). In unvegetated sediments, increasing inundation weakened the relative dominance of DNF and increased the importance of DNRA. Across the 0–65 % mean inundation-frequency gradient, DNF contribution declined from approximately 62 % to 48 %, whereas DNRA contribution increased from 25 % to 34 % (Fig. 3d). DNF nevertheless remained the largest NO_3^--reduction pathway even under the highest inundation, indicating a strong hydrological forcing redirected NO_3^- fate toward greater DNRA-mediated nitrogen retention.

This pathway rebalancing occurred along a pronounced hydrological–redox gradient. Increasing inundation was accompanied by higher sediment water content and declining ORP, consistent with restricted oxygen diffusion and prolonged reducing conditions in waterlogged sediments (Fig. 2; Table 1). This pattern is consistent with the general understanding that waterlogging restricts oxygen diffusion and prolongs anaerobic exposure in wetland sediments (Gao et al., 2024; Zhai et al., 2018). The importance of this hydrologically imposed redox gradient was further supported by the RF analysis, which identified ORP and sediment water content as key predictors of DNF% (Fig. 6b). This redox-based interpretation is consistent with recent evidence from mangrove sediments showing that DNF is favored in shallower and more oxidized layers, whereas DNRA becomes increasingly important with depth and stronger reducing conditions (Fan et al., 2024). However, redox state alone is unlikely to determine whether NO_3^- is ultimately reduced through DNF or DNRA.

The DNF - DNRA partitioning depends not only on redox conditions, but also on the relative supply of electron donors and acceptors, NO_3^-/NO_2^- availability, microbial growth strategies, and electron-donor identity (Kraft et al., 2014; van der Putten et al., 2016; Yoon et al., 2015). Experimental studies show that denitrification tends to gain a competitive advantage under electron-donor limitation, whereas respiratory ammonification becomes more favorable when electron acceptors are limiting relative to available reducing equivalents. Moreover, fermentable substrates can alter this competition by generating reduced intermediates and redistributing electron donors between fermenters and NO_3^- reducers. In our experiment, bulk DOC and NO_3^- concentrations showed no significant elevational differences in the CK treatment (Fig. 2d–f; $p > 0.05$), and PLS-SEM analysis indicated only a weak direct effect of the DOC: NO_3^- ratio on DNF-DNRA pathway balance (0.03). This weak bulk-substrate effect may be partly explained by the marsh-organ platform operated as an open estuarine system subject to tidal exchange. The observed pathway divergence likely reflected redox-mediated reorganization of microbial electron flow and substrate use, rather than simple changes in bulk substrate pools.

Our MAG-resolved data further support a resource-use interpretation of DNF–DNRA competition. DNRA-associated MAGs more frequently

contained genes related to H_2 metabolism and acetate/ethanol utilization, whereas respiratory and oxidative energy-metabolism modules were more strongly represented among DNF-associated MAGs (Fig.5& Table S7). This pattern is consistent with experimental evidence that electron-donor identity and fermentability can alter DNF–DNRA competition by changing the substrates available to NO_3^- reducers; for example, fermentation can generate acetate and redistribute electron donors among fermenters, denitrifiers, and DNRA bacteria (van den Berg et al., 2017b). Recent physiological evidence further demonstrates that H_2 can directly support DNRA through hydrogenase-mediated electron transfer, providing a plausible basis for the greater representation of H_2-metabolism potential in DNRA-associated MAGs (Handler et al., 2022). These metabolic traits are consistent with greater representation of fermentation-coupled resource-use potential under stronger inundation. However, because H_2, volatile fatty acids, and other labile electron donors were not measured directly, these genomic patterns should be interpreted as contrasting metabolic potentials rather than evidence that any specific substrate controlled DNF–DNRA partitioning in situ.

Therefore, prolonged inundation likely increased the competitive importance of DNRA-associated nitrogen retention by creating a reducing metabolic background favorable to fermentative and reductive NO_3^--reducing assemblages. The secondary contribution of ANA may partly reflect its additional dependence on simultaneous NH_4^+ and NO_2^- availability (Babbin et al., 2015; Hou et al., 2015). Under our $^{15}NO_3^-$ incubation conditions, ANA relied on NO_2^- generated during NO_3^- reduction, which may have constrained its contribution relative to DNF and DNRA.

4.2. Plant survival modifies inundation-driven NO_3^- reduction pathways

Against the gradual hydrological response observed in unvegetated sediments, planted sediments showed a markedly nonlinear reorganization of NO_3^--reduction pathways. Model analysis identified a hydrological transition around 24 % mean inundation frequency, supported by the nonlinear responses of DNRA rate, DNRA contribution, and DNF–DNRA pathway balance (Fig. S4 & Table S7). Importantly, this transition was driven primarily by the rapid increase in DNRA importance rather than by an abrupt loss of DNF, which remained substantial under the highest inundation frequency. A. marina survived at elevations ≥50 cm (0–28 % mean inundation frequency) but failed to establish at 0 and −50 cm (47–65 % mean inundation frequency), with biomass peaking at 150 cm. Where plants persisted, DNF contribution reached up to ~85 % and DNRA generally remained low, whereas DNRA approached 48 % under the strongest inundation where plants failed. Importantly, the observed plant-survival boundary (28–47 % mean inundation frequency) did not coincide exactly with the 24 % nitrogen-process transition, indicating that plant persistence modified the nonlinear pathway response.

Consistent with this interpretation, plant survival coincided with differences in sediment redox status. Mangrove seedlings are sensitive to prolonged waterlogging and oxygen limitation (Colmer and Voesenek, 2009; Liao, 2010), but surviving mangroves can transport oxygen to belowground tissues and partially buffer reducing rhizosphere conditions through root-mediated oxygen transport and radial oxygen loss (Cheng et al., 2020; Gao et al., 2025; McKee, 1996). Consistent with this mechanism, ORP within planted sediments increased from −54.7 mV at the most strongly inundated elevation to >280 mV at elevations ≥100 cm. However, Plant–CK differences in ORP varied among elevations rather than showing a uniformly positive planting effect, suggesting that vegetation modified sediment redox conditions in a hydrologically dependent manner. Thus, plant persistence may have buffered the reducing effects of inundation locally, whereas this live-root influence was weakened or absent where plant establishment failed.

Microbial functional patterns further support the plant-survival-associated amplification of the DNF–DNRA pathway divergence across the inundation threshold. RDA and MAG-resolved analyses showed that microbial metabolic differentiation was closely associated with plant biomass (Fig. 6a). Within the high-biomass range of 50–150 cm, planted sediments were enriched in DNF-associated assemblages, including Pseudomonas and Paracoccus (Fig. 4a). DNF-related MAGs aligned with oxidative carbon metabolism and respiratory energy metabolism modules, such as *nuoAB* and *ccoNOP*, suggesting that sediments with surviving plants had microbial functional potentials favorable to DNF (Fig. 5) (Kraft et al., 2014). In contrast, sediments where plants failed under strong inundation were associated with DNRA-favorable microbial traits, including fermentative and reductive carbon metabolism. Plant failure may have further increased the availability of reduced organic substrates through decomposition (van den Berg et al., 2017a), thereby reinforcing DNRA-mediated nitrogen retention under strongly reducing conditions. Overall, these patterns suggest that hydrology constrained plant survival, while surviving plants were associated with less reducing sediment conditions and microbial functional potentials favorable to DNF.

Statistical analyses further support this interpretation. Effect-size analysis showed that planting exerted a particularly strong influence on potential DNF, whereas elevation had a stronger effect on DNRA; the substantial elevation × planting interaction for DNF further indicated that the vegetation effect depended on hydrological context (Table 1). The PLS-SEM was consistent with this pattern, linking inundation primarily to sediment moisture and redox conditions, while plant biomass contributed to DNF–DNRA pathway balance through both direct and environmentally mediated associations (Fig. 6c,d). Microbial gene indicators provided comparatively limited additional explanatory power (Fig.S5 & Table S5). Together, these results suggest that inundation establishes the environmental template for nitrate-reduction partitioning, whereas vegetation–sediment feedbacks modify and amplify the pathway response within that hydrological constraint.

4.3. Implications for coastal water quality and mangrove restoration

Hydrological regulation of sediment nitrogen cycling has been widely observed in tidal wetlands. Previous studies have shown that changes in flooding frequency alter denitrification through associated changes in sediment moisture, redox conditions, plant performance, and microbial communities (Bai et al., 2017; Hu et al., 2019). However, these studies generally characterized hydrology using flooding-frequency classes or experimental flooding treatments rather than the proportion of time inundated, and they did not identify a comparable DNF–DNRA transition point. Our results extend this understanding by showing that inundation regulates not only the magnitude of NO_3^- reduction but also its partitioning between DNF-mediated nitrogen removal and DNRA-mediated nitrogen retention (Burgin and Hamilton, 2007; Zhang et al., 2023). This pathway rebalancing is particularly relevant to coastal water quality because it determines whether reactive nitrogen is removed from or retained within the wetland system.

This finding has direct implications for mangrove restoration. Restoration outcomes should not be inferred from vegetation establishment or inundation intensity alone. Instead, sediment elevation relative to tidal inundation should be considered when evaluating whether restored mangrove wetlands can sustain DNF-favorable sediment conditions (Gao et al., 2025; Spencer et al., 2016). Placing mangroves below suitable inundation ranges may limit plant survival, weaken redox buffering, and favor DNRA-mediated nitrogen retention rather than DNF-mediated NO_3^- removal (Fig. 3d). Therefore, restoration and management strategies should account for inundation regime, sediment elevation, plant survival, and DNF–DNRA partitioning when assessing the nitrogen-filtering capacity of mangrove wetlands under climate- and human-driven hydrological change.

The 24 % hydrological transition in mean inundation frequency

identified here should be viewed as a system-specific environmental boundary for this *A. marina* marsh-organ system, not a universal mangrove growth threshold. Because the isotope incubations quantified potential DNF–ANA–DNRA partitioning rather than complete ^{15}N mass balance, future work should combine in situ N fluxes, N_2O measurements, rhizosphere-scale redox observations, and cross-regional comparisons to test the transferability of this framework.

5. Conclusion

This study shows that inundation regulates NO_3^- reduction pathways in mangrove sediments, while plant survival modifies the form of this hydrological response. In unvegetated sediments, high inundation weakened DNF dominance and increased DNRA importance, whereas planted sediments exhibited a nonlinear transition at approximately 24 % mean inundation frequency. This transition was accompanied by contrasting redox conditions and microbial functional traits associated with plant survival and failure. Together, these findings indicate that nitrogen removal in mangrove wetlands cannot be inferred from inundation intensity or vegetation establishment alone. Instead, restoration performance depends on the coupling among sediment elevation, inundation regime, plant survival, and NO_3^-reduction pathways. The ~24 % transition should therefore be viewed as a system-specific expression of coupled hydrological, plant, and microbial regulation rather than a universal threshold. These findings provide a process-based basis for evaluating how altered inundation regimes may weaken nitrogen removal and enhance nitrogen retention in mangrove wetlands.

CRediT authorship contribution statement

Shiyao Chen: Writing – review & editing, Writing – original draft, Visualization, Methodology, Investigation, Formal analysis, Data curation, Conceptualization. **Hui Wu:** Writing – review & editing, Investigation, Data curation. **Yasong Chen:** Writing – review & editing, Investigation, Data curation. **Fenfang Wang:** Writing – review & editing, Methodology, Conceptualization. **Yihui Zhang:** Writing – review & editing, Methodology. **Nengwang Chen:** Writing – review & editing, Supervision, Project administration, Methodology, Funding acquisition, Conceptualization.

Declaration of competing interest

The authors declare that they have no known competing financial interests or personal relationships that could have appeared to influence the work reported in this paper.

Acknowledgements

This work was supported by the National Natural Science Foundation of China (422706011), the National Key R&D Program of China (2022YFF0802102), the National Natural Science Foundation of China (42530405), and MEL Internal Program (No. MELRI2501). We are grateful to Wenhong Xu, Wenyan Tang, Mengru Li, Yuanhao Cao, Chunyan Cheng, Ting Jiang, and Yuyang Zheng for their help in field measurement, and to Liyang Zhan, Junhui Chen, Fang Wu, Junou Du, and Lei Wang for their supportive technician work.

Supplementary materials

Supplementary material associated with this article can be found, in the online version, at doi:10.1016/j.watres.2026.126911.

Data availability

Data will be made available on request.

References

Alldred, M., Baines, S.B., 2016. Effects of wetland plants on denitrification rates: a meta-analysis. Ecol. Appl. 26 (3), 676–685.
An, S., Gardner, W.S., 2002. Dissimilatory nitrate reduction to ammonium (DNRA) as a nitrogen link, versus denitrification as a sink in a shallow estuary (Laguna Madre/Baffin Bay, Texas). Mar. Ecol. Prog. Ser. 237, 41–50.
Babbin, A.R., Jayakumar, A., Ward, B.B., 2016. Organic matter loading modifies the microbial community responsible for nitrogen loss in estuarine sediments. Microb. Ecol. 71 (3), 555–565.
Bai, J., Wang, X., Jia, J., Zhang, G., Wang, Y., Zhang, S., 2017. Denitrification of soil nitrogen in coastal and inland salt marshes with different flooding frequencies. Phys. Chem. Earth 97, 31–36.
Ballantine, K.A., Groffman, P.M., Lehmann, J., Schneider, R.L., 2014. Stimulating nitrate removal processes of restored wetlands. Environ. Sci. Technol. 48 (13), 7365–7373.
Booth, J.M., Fusi, M., Marasco, R., Daffonchio, D., 2023. The microbial landscape in bioturbated mangrove sediment: a resource for promoting nature-based solutions for mangroves. Microb. Biotechnol. 16 (8), 1584–1602.
Buchfink, B., Xie, C., Huson, D.H., 2015. Fast and sensitive protein alignment using Diamond. Nat. Methods 12, 59–60.
Burgin, A.J., Hamilton, S.K., 2007. Have we overemphasized the role of denitrification in aquatic ecosystems? A review of nitrate removal pathways. Front. Ecol. Environ. 5 (2), 89–96.
Cai, H., Zhang, X., Zhang, M., Guo, L., Liu, F., Yang, Q., 2019. Impacts of Three Gorges Dam's operation on spatial–temporal patterns of tide–river dynamics in the Yangtze River estuary, China. Ocean Sci. 15 (3), 583–599.
Cheng, H., Liu, Y., Jiang, Z.Y., Wang, Y.S., 2020. Radial oxygen loss is correlated with nitrogen nutrition in mangroves. Tree Physiol. 40 (11), 1548–1560.
Colmer, T.D., Voesenek, L.A.C.J., 2009. Flooding tolerance: suites of plant traits in variable environments. Funct. Plant Biol. 36, 665–681.
Davidson, E.A., Seitzinger, S., 2006. The Enigma of Progress in denitrification research. Ecol. Appl. 16 (6), 2057–2063.
Elsey-Quirk, T., Graham, S.A., Mendelssohn, I.A., Snedden, G., Day, J.W., Twilley, R.R., Shaffer, G., Sharp, L.A., Pahl, J., Lane, R.R., 2019. Mississippi river sediment diversions and coastal wetland sustainability: synthesis of responses to freshwater, sediment, and nutrient inputs. Estuar. Coast. Shelf Sci. 221, 170–183.
Fan, Y., Zhou, Z., Liu, F., Qian, L., Yu, X., Huang, F., Hu, R., Su, H., Gu, H., Yan, Q., He, Z., Wang, C., 2024. The vertical partitioning between denitrification and dissimilatory nitrate reduction to ammonium of coastal mangrove sediment microbiomes. Water Res. 262, 122113.
Gao, G.-F., Song, L., Zhang, Y., Chu, H., 2024. Expedited loss of soil biodiversity in blue carbon ecosystems caused by rising sea levels. Soil Biol. Biochem. 191.
Gao, T., Li, Y., Yang, N., Xiong, W., Liang, X., Wang, Y., 2025. Plant-rhizosphere microbe interactions and their roles in nitrogen cycles under periodic flooding: from cooperation mechanisms to ecological responses. Crit. Rev. Environ. Sci. Tec. 55 (17), 1358–1382.
Handler, A.M., Suchy, A.K., Grimm, N.B., 2022. Denitrification and DNRA in Urban accidental wetlands in Phoenix, Arizona. J. Geophys. Res. Biogeosci. 127 (2).
Hou, L., Yin, G., Liu, M., Zhou, J., Zheng, Y., Gao, J., Zong, H., Yang, Y., Gao, L., Tong, C., 2015. Effects of sulfamethazine on denitrification and the associated N_2O release in estuarine and coastal sediments. Environ. Sci. Technol. 49 (1), 326–333.
Hou, L., Zheng, Y., Liu, M., Li, X., Lin, X., Yin, G., Gao, J., Deng, F., Chen, F., Jiang, X., 2015. Anaerobic ammonium oxidation and its contribution to nitrogen removal in China's coastal wetlands. Sci. Rep. 5 (1).
Hu, W., Zhang, W., Zhang, L., Lin, X., Tong, C., Lai, D.Y.F., Chen, Y., Zeng, C., 2019. Short-term changes in simulated inundation frequency differentially affect inorganic nitrogen, nitrification, and denitrification in estuarine marshes. Ecol. Indic. 107.
Huang, H.Z., Guo, Z.Y., Zhang, Y.C., Jin, L., Zhuang, L.H., Chen, L.J., Zheng, H.X., Hong, X.Y., Tang, H.C., Liu, J.K., Zheng, H.L., Zhu, X.Y., 2026. Salt excretion: a new function of lenticels on pneumatophores of the mangrove Avicennia marina. New. Phytol. 250, 2288–2303.
Koyama, T., Enggrob, K.L., Rasmussen, J., Martins, J.T., Peixoto, L., 2025. Substrate quantity and quality affect microbial carbon use efficiency and priming effects of root exudates investigated with microdialysis. Soil Biol. Biochem. 209, 109869.
Kraft, B., Tegetmeyer, H.E., Sharma, R., Klotz, M.G., Ferdelman, T.G., Hettich, R.L., Geelhoed, J.S., Strous, M., 2014. The environmental controls that govern the end product of bacterial nitrate respiration. Science 345 (6197), 676–679.
Kristensen, E., Bouillon, S., Dittmar, T., Marchand, C., 2008. Organic carbon dynamics in mangrove ecosystems: a review. Aquat. Bot. 89 (2), 201–219.
Li, X., Gao, D., Hou, L., Liu, M., 2019. Salinity stress changed the biogeochemical controls on CH_4 and N_2O emissions of estuarine and intertidal sediments. Sci. Total Environ. 652, 593–601.
Li, X., Qian, W., Hou, L., Liu, M., Chen, Z., Tong, C., 2020. Soil organic carbon controls dissimilatory nitrate reduction to ammonium along a freshwater-oligohaline gradient of Min River Estuary. Mar. Pollut. Bull. 160, 111696.
Liao, B. (2010) The adaptability of seedlings of three mangrove species to tide-flooding and water salinity Chinese Academy of Forestry, Beijing, China.
Lu, Z., Xiao, K., Wang, F., Wang, Y., Yu, Q., Chen, N., 2023. Salt marsh invasion reduces recalcitrant organic carbon pool while increases lateral export of dissolved inorganic carbon in a subtropical mangrove wetland. Geoderma 437, 116573.
Ma, T.-F., Yu, X.-Y., Xing, C.-Y., Liu, Z., Wu, Z.-J., Chen, Y.-P., 2025. Nitrogen recovery through dissimilatory nitrate reduction to ammonium: impact of environmental factors. ACS Omega 10 (16), 16695–16704.
McKee, K.L., 1996. Growth and physiological responses of neotropical mangrove seedlings to root zone hypoxia. Tree Physiol. 16, 883–889.

Nedwell, D.B., 1975. Inorganic nitrogen metabolism in a eutrophicated tropical mangrove estuary. Water Res. 9 (2), 221–231.
Peng, D., Chen, L., Pennings, S.C., Zhang, Y., 2018. Using a marsh organ to predict future plant communities in a Chinese estuary invaded by an exotic grass and mangrove. Limnol. Oceanogr. 63 (6), 2595–2605.
Spencer, T., Schuerch, M., Nicholls, R.J., Hinkel, J., Lincke, D., Vafeidis, A.T., Reef, R., McFadden, L., Brown, S., 2016. Global coastal wetland change under sea-level rise and related stresses: the DIVA wetland Change Model. Global Planet. Change 139, 15–30.
Tahsin, S., Medeiros, S.C., Singh, A., 2018. Assessing the resilience of coastal wetlands to extreme hydrologic events using vegetation indices: a review. Remote Sens. 10 (9), 1390.
Uritskiy, G.V., DiRuggiero, J., Taylor, J., 2018. MetaWRAP—A flexible pipeline for genome-resolved metagenomic data analysis. Microbiome 6 (1), 158.
van den Berg, E.M., Elisario, M.P., Kuenen, J.G., Kleerebezem, R., van Loosdrecht, M.C. M., 2017a. Fermentative bacteria influence the competition between denitrifiers and DNRA bacteria. Front. Microbiol. 8, 1684.
van den Berg, E.M., Elisario, M.P., Kuenen, J.G., Kleerebezem, R., van Loosdrecht, M.C. M., 2017b. Fermentative bacteria influence the competition between denitrifiers and DNRA bacteria. Front. Microbiol. 8, 1684.
van der Putten, W.H., Bradford, M.A., Pernilla Brinkman, E., van de Voorde, T.F.J., Veen, G.F., Bailey, J.K., 2016. Where, when and how plant–soil feedback matters in a changing world. Funct. Ecol. 30 (7), 1109–1121.
Voss, C.M., Christian, R.R., Morris, J.T., 2013. Marsh macrophyte responses to inundation anticipate impacts of sea-level rise and indicate ongoing drowning of North Carolina marshes. Mar. Biol. 160 (1), 181–194.
Wang, F., Lu, Z., Tobias, C.R., Wang, Y., Xiao, K., Yu, Q., Lin, J., Huang, G., Chen, N., 2023. Salt marsh expansion into estuarine mangrove mudflats reduces nitrogen removal capacity. Catena 232, 107459.
Wang, J., Chen, X., Wang, Y., Chen, Y., Wu, H., Wittyngham, S.S., Kirwan, M.L., Zhang, Y., Liu, W., Zhang, Y., 2025. Life-history plasticity of intertidal salt marsh in response to sea level rise: salinity and inundation modulate size-dependent flowering of Spartina alterniflora. Ecol. Indic. 177, 113790.
Wang, W., Fu, H., Lee, S.Y., Fan, H., Wang, M., 2020. Can strict protection stop the decline of mangrove ecosystems in China? From rapid destruction to rampant degradation. Forests 11 (1), 55.
Wilson, S.J., Megonigal, J.P., 2025. Nitrate reduction across soils transitioning from coastal forest to wetland are hotspots for denitrification. Soil Biol. Biochem. 209, 109904.
Yin, G., Hou, L., Liu, M., Zheng, Y., Li, X., Lin, X., Gao, J., Jiang, X., 2016. Effects of thiamphenicol on nitrate reduction and N_2O release in estuarine and coastal sediments. Environ. Pollut. 214, 265–272.
Yoon, S., Cruz-García, C., Sanford, R., Ritalahti, K.M., Löffler, F.E., 2015. Denitrification versus respiratory ammonification: environmental controls of two competing dissimilatory NO_3^-/NO_2^- reduction pathways in Shewanella loihica strain PV-4. ISME J. 9 (5), 1093–1104.
Zhai, S., Ji, M., Pavlostathis, S.G., Zhao, Y., 2019. Impact of hydraulic retention time and current on the microbial community and denitrification genes in a continuous-flow biofilm electrode reactor. J. Chem. Technol. Biot. 94 (3), 933–941.
Zhang, X., Yao, C., Zhang, B., Tan, W., Gong, J., Wang, G.-Y., Zhao, J., Lin, X., 2023. Dynamics of benthic nitrate reduction pathways and associated microbial communities responding to the development of seasonal deoxygenation in a coastal mariculture zone. Environ. Sci. Technol. 57 (40), 15014–15025.
Zhao, L., Chen, J., Shen, G., Zhou, Y., Zhang, X., Zhou, Y., Yu, Z., Ma, J., 2025. Dissimilatory nitrate reduction to ammonia in the natural environment and wastewater treatment facilities: a comprehensive review. Environ. Technol. Innov. 37, 104011.
Zhijiang, S., Tao, W., Yunxia, Z., Bin, Z., 2020. Effect of wet and dry alternation on denitrification in natural ditch sediments. Acta Sci. Circumst. 40 (11), 4010–4017.
Zhou, Z., Tran, P.Q., Breister, A.M., Liu, Y., Kieft, K., Cowley, E.S., Karaoz, U., Anantharaman, K., 2022. METABOLIC: high-throughput profiling of microbial genomes for functional traits, metabolism, biogeochemistry, and community-scale functional networks. Microbiome 10 (1), 33.